

Railway alignment optimization in regions with densely-distributed obstacles based on semantic topological maps

Xinjie Wan^{a,b}, Hao Pu^{a,b,*}, Paul Schonfeld^c, Taoran Song^{a,b}, Wei Li^{a,b} and Lihui Peng^d

^a*School of Civil Engineering, Central South University, Changsha, Hunan, China*

^b*National Engineering Research Center of High-speed Railway Construction Technology, Changsha, Hunan, China*

^c*Department of Civil and Environmental Engineering, University of Maryland, College Park, MD, USA*

^d*China Railway Siyuan Survey and Design Group Co. Ltd, Wuhan, Hubei, China*

Abstract. Railway alignment development in a study area with densely-distributed obstacles, in which regions favorable for alignments are isolated (termed an isolated island effect, i.e., IIE), is a computation-intensive and time-consuming task. To enhance search efficiency and solution quality, an environmental suitability analysis is conducted to identify alignment-favorable regions (AFRs), focusing the subsequent alignment search on these areas. Firstly, a density-based clustering algorithm (DBSCAN) and a specific criterion are customized to distinguish AFR distribution patterns: continuously-distributed AFRs, obstructed effects, and IIEs. Secondly, a study area characterized by IIEs is represented with a semantic topological map (STM), integrating between-island and within-island paths. Specifically, between-island paths are derived through a multi-directional scanning strategy, while within-island paths are optimized using a Floyd-Warshall algorithm. To this end, the intricate alignment optimization problem is simplified into a shortest path problem, tackled with conventional shortest path algorithms (of which Dijkstra's algorithm is adopted in this work). Lastly, the proposed method is applied to a real case in a mountainous region with karst landforms. Numerical results indicate its superior performance in both construction costs and environmental suitability compared to human designers and a prior alignment optimization method.

Keywords: Railway design, alignment optimization, geographic analysis, constrained optimization, semantic topological map

1. Introduction

Railway alignment design is a complicated process, which aims to determine the railway geometric profiles [1,2] and structure configurations [3,4] between two given points. This process takes into account various factors such as topographic [5,6] and geologic [7] conditions, alongside numerous hard-to-quantify objectives [8,9]. Currently, this iterative and time-consuming railway design process is still mainly conducted by human designers. However, due to fi-

nite time and resources, several promising alignment alternatives may still be overlooked, especially when alignment-favorable regions (AFRs) are sparse in the study area. Optimizing an alignment in such cases requires substantial time and effort. To enhance the alignment generation efficiency and solution quality, many computer-aided approaches have been proposed for automatically optimizing alignments between two given points [10,11].

Alignment determination is inherently an optimization problem, comprising three essential components: objective functions, design variables and constraints. The objective function is a mathematical expression of alignment fitness in terms of various factors, such as construction costs, geologic and ecologic conditions [12]. An alignment is typically described as a se-

*Corresponding author: Hao Pu, National Engineering Research Center of High-speed Railway Construction Technology, Changsha 410075, Hunan, China. E-mail: haopu@csu.edu.cn

27 quence of points of intersection (PIs) and their corre-
28 sponding curve sections [13]. Therefore, the geometric
29 parameters of alignment PIs and curves are defined as
30 the design variables [14]. Constraints are imposed for
31 ensuring that alignments adhere to railway design crite-
32 ria, construction limitations, and their relative positions
33 to other ground features [15].

34 Most alignment optimization methods can be catego-
35 rized into two main types: nature-inspired methods and
36 shortest-path methods. These classifications are based
37 on the evolutionary mechanism of the PIs.

- 38 (1) In nature-inspired alignment optimization meth-
39 ods, all PIs are generated at the initial stage and
40 iteratively adjusted according to the alignment
41 fitness, considering various costs and impacts.
42 Once the iterative adjustment process converges,
43 the selected PIs determine an optimized align-
44 ment. Several effective nature-inspired meth-
45 ods have been applied in optimizing highway
46 and railway alignments, such as genetic algo-
47 rithms (GA) [16,17], particle swarm optimiza-
48 tion (PSO) [18,19] and ant colony optimization
49 (ACO) [20,21]. In addition, hybrid optimiza-
50 tion methods that integrate two or more nature-
51 inspired approaches, such as a GA-ACO [22] and
52 a PSO-GA [23], have been proposed for outper-
53 forming non-hybrid methods in alignment opti-
54 mization.
- 55 (2) Shortest-path alignment optimization methods
56 involve selecting and accumulating the best PIs
57 within local ranges to form a complete align-
58 ment. Various approaches have been used in
59 shortest-path alignment optimization, including
60 grid-based methods using distance transforms
61 (DT) [24,25], graph-based methods using Di-
62 jkstra's algorithms [26,27] and sampling-based
63 methods using rapidly exploring random tree al-
64 gorithms (RRT) [28,29]. These methods have
65 proven successful in solving alignment optimiza-
66 tion problems.

67 In nature-inspired alignment optimization methods,
68 the fixed number of PIs during the alignment search
69 process limits their application in complex alignment
70 design spaces. This rigidity arises from the need to ad-
71 just the number of PIs flexibly, particularly when navi-
72 gating densely-distributed obstacles. On the other hand,
73 shortest-path algorithms yield outcomes comprising
74 piecewise line segments, necessitating further adjust-
75 ments into a detailed alignment solution. This involves
76 configuring curve sections and determining structure

77 layouts, thereby deviating from the initially optimized
78 path.

79 Given the limitations of these methods, researchers
80 have sought to combine them to tackle alignment opti-
81 mization problems in intricate study areas. Drawing in-
82 spiration from the area-corridor-alignment design phi-
83 losophy employed by human designers, Li et al. [26]
84 customized DT to generate paths, represented as piece-
85 wise line segments, during the area-corridor design
86 stage. They then utilized a GA to refine the alignment
87 alternatives in the corridor-alignment design stage. Fur-
88 thermore, Karlson et al. [8] developed a bi-objective
89 optimization model for railway corridor planning that
90 accounted for ecologic and geologic factors. Mondal
91 et al. [30] adopted a combination approach, utilizing a
92 derivative-free optimization method (NOMAD) along
93 with a parallel search package to generate horizontal
94 alignments within a predefined corridor.

95 All the alignment optimization methods mentioned
96 above are based on some iterative process, where con-
97 straints are checked and handled during the search pro-
98 cess in which an alignment is deemed infeasible if it vi-
99 olates any considered constraints [31]. However, these
100 methods face challenges in study areas with densely-
101 distributed obstacles, where feasible alignment regions
102 are significantly squeezed and fragmented by multi-
103 ple obstacles. This results in inefficient exploration of
104 alignment-unfavorable regions, consuming substantial
105 computing resources and time.

106 Several obstacle preprocessing methods have been
107 developed in the motion planning field to address
108 these challenges. Li et al. [32] abstracted obstacles as
109 hexagons, constructing a feasible path network by con-
110 necting selected vertexes from these hexagons. Paths
111 were considered infeasible if the line connecting adja-
112 cent vertexes intersected obstacles. Hu et al. [33] de-
113 veloped a Voronoi Diagram (VD) based on obstacles
114 and subsequent path optimization was applied to this
115 VD. While these methods shed new light on obstacle
116 handling strategies, generating satisfactory solutions
117 in areas with densely-distributed obstacles remained
118 challenging, particularly if all obstacles were treated as
119 forbidden regions.

120 To address this problem, Pu et al. [34] have abstracted
121 the study area as a grid set and performed environ-
122 mental suitability evaluation on these grid cells. Af-
123 terward, the AFRs are identified, and the subsequent
124 alignment search process focuses on these regions. In
125 Pu et al. [34], a connecting patch of AFRs envelops the
126 start and end points, creating a pattern characterized by
127 continuously-distributed AFRs across the study area. In

128 this case, the existing alignment optimization methods
129 can efficiently produce optimized alignments with the
130 assistance of the environmental suitability analysis [34].

131 As China's railway construction environment grows
132 increasingly complex and research progresses, the au-
133 thors' team has found that in regions characterized by
134 undulating terrains, AFRs include obstructions such
135 as high mountains or deep valleys [35]. This poses a
136 significant challenge in devising optimized layouts for
137 dominating structures (i.e., deep-buried long tunnels
138 and large-span high bridges) using traditional alignment
139 optimization methods. Thus, Wan et al. [35] developed
140 a bi-level optimization model for determining domi-
141 nating structures at the upper level and optimizing the
142 complete alignments at the lower-level. According to
143 the characteristics of the distribution pattern of AFRs,
144 study areas with the above-mentioned conditions are
145 referred to as obstructed effects in this paper.

146 In recent years, as China's railway network contin-
147 ued to expand and improve, several real-world rail-
148 way scenarios have presented substantial challenges
149 to alignment design. For example, in a section of the
150 Shanghai-Chongqing-Chengdu High-speed Railway,
151 karst hazards dominate almost 90% of the study area.
152 This widespread presence of geo-hazards, coupled with
153 ecologically sensitive regions, creates an alignment
154 search space densely packed with obstacles. Moreover,
155 urban high-speed railways increasingly contend with
156 complex networks, such as existing roads and rivers,
157 along with planar constraints such as existing buildings
158 and water conservation zones. These constraints result
159 in severe fragmentation of feasible regions available for
160 traversing alignments.

161 Given this landscape, existing computer-aided align-
162 ment optimization methods face considerable difficul-
163 ties in efficiently generating satisfactory alignment so-
164 lutions. Ensuring solution quality while accommodating
165 numerous constraints becomes a daunting task within
166 such intricate and constrained environments.

167 Given the increasing complexity of China's rail-
168 way construction environment and the prevalence of
169 study areas with densely-distributed obstacles, there is
170 a growing need to overcome the limitations imposed on
171 alignment optimization efficiency and quality by IIEs.
172 Consequently, this paper introduces a completely new
173 alignment optimization framework tailored to address
174 the intricate alignment optimization challenges encoun-
175 tered in study areas with IIEs. Notably, given the com-
176 plexity of this challenge, this study primarily focuses
177 on generating alignment corridor alternatives during the
178 area-corridor design stage. These alternatives serve as

179 initial optimized corridors for subsequent stages, par-
180 ticularly the corridor-alignment stage. It is important to
181 highlight that while the existing alignment optimization
182 methods can efficiently address the optimization prob-
183 lems at the corridor-alignment stage, this paper does
184 not focus on this aspect.

185 The main contributions of this work are summarized
186 as follows:

- 187 (1) An environmental suitability analysis and a DB-
188 SCAN clustering algorithm are performed on
189 the study area before alignment search process
190 for capturing the distribution characteristics of
191 AFRs, as shown in Fig. 1. Subsequently, a spe-
192 cific criterion is developed to differentiate be-
193 tween IIEs and the other two AFRs distribution
194 patterns, namely continuously-distributed AFRs
195 and obstructed effects.
- 196 (2) The IIEs in the study area are abstracted as a
197 semantic topological map (STM) for facilitat-
198 ing a subsequent path generation stage. Specifi-
199 cally, between-island paths are generated based
200 on the relative locations of AFRs and through
201 a designed multi-directional scanning process.
202 Meanwhile within-island paths are determined
203 using the endpoints of between-island paths and
204 a conventional Floyd-Warshall algorithm. To this
205 end, alignment optimization problem in the study
206 area with densely-distributed obstacles is trans-
207 formed into a shortest path problem on a graph.
208 Consequently, this can efficiently generate op-
209 timized paths using conventional shortest path
210 algorithms, such as Dijkstra's, which is adopted
211 in this paper.

212 The remainder of this work is organized as follows:
213 Section 2 presents the land parcel preprocessing proce-
214 dures. Section 3 introduces the construction process of
215 the STM. Section 4 shows the alignment optimization
216 method. Section 5 provides a realistic case study and
217 Section 6 concludes this study.

218 **2. Land parcel preprocessing**

219 *2.1. Environmental suitability analysis for alignments*

220 First, according to the resolution of the digital ele-
221 vation model (DEM) used at the area-corridor railway
222 design stage [36,37], the study area is abstracted into a
223 set of grid cells. Ground elevations, geo-hazard regions
224 and unit structural costs are then stored in each grid cell,
225 forming the essential railway design data. Subsequently,

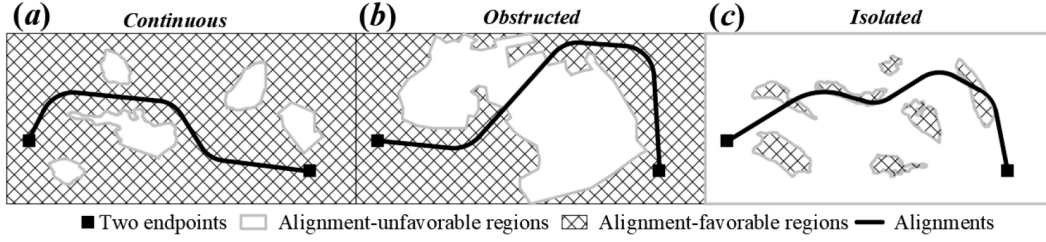


Fig. 1. Three different land parcel distribution patterns: AFRs are (a) continuous; (b) obstructed and (c) isolated.

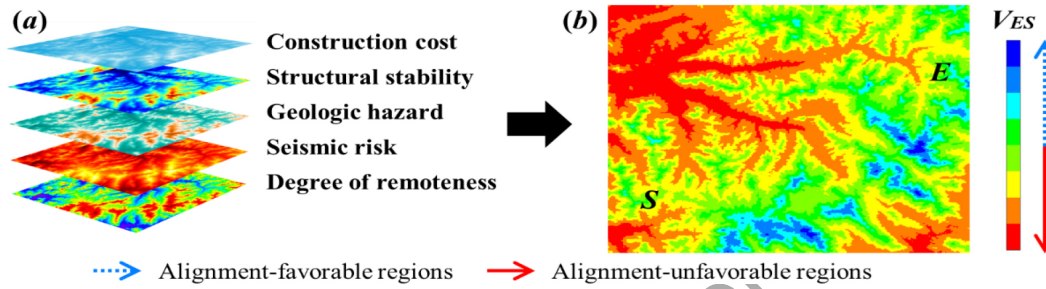


Fig. 2. (a) Environmental suitability influential factors and (b) environmental suitability map for alignments.

an environmental suitability analysis for alignments is conducted on this grid set [37]. In Pu et al. [37], multiple topographic and geologic factors are integrated to determine an environmental suitability value (V_{ES}) for each grid cell. The evaluation of a grid cell's environmental suitability accounts for the impacts of construction cost, stability, geologic hazard and seismic risk for different railway structures, as well as the degree of remoteness:

$$V_{ES} = \sum_{i=1}^5 (\omega_i \cdot x_i) \quad (1)$$

where x_i is the nondimensionalized value (i.e., ranging from 0 to 1) for the construction cost, stability, geologic hazard, seismic risk or degree of remoteness for the grid cell and ω_i is the criterion weight for the i th influencing factor. It is noteworthy that the relative significance of different indicators is determined using a multi-criteria decision-making method known as CRITIC (criteria importance through inter-criteria correlation). This method involves assigning weights to various indicators based on their values across the entire study area. Indicators exhibiting higher variance and lower correlation are assigned higher weights. Detailed formulations can be found in Pu et al. [37].

Figure 2 displays an environmental suitability map for alignments, where grid cells with higher V_{ES} values are considered preferable for traversing alignments. To distinguish between alignment-favorable and unfavor-

able regions, an environmental suitability threshold for alignments (T_{ES}) is assigned. Grid cells with V_{ES} values exceeding the T_{ES} are classified as alignment-favorable grid cells (AFGs), while the remaining grid cells constitute alignment-unfavorable grid cells (AUGs). The threshold value assigned to AFGs and AUGs plays a critical role in establishing the distribution pattern of AFGs. In this paper, the threshold is determined based on the environmental suitability value corresponding to the inflection point (P_{in}) of the cumulative probability distribution curve ($F(x)$). The curve $F(x)$ is constructed by fitting the cumulative frequency of each distinct V_{ES} value in ascending order. The frequency ($F(x_i)$) of the i th V_{ES} value is formulated according to Eq. (2).

$$F(x_i) = \frac{\sum_{j=1}^i F_{ESj}}{N} \quad (2)$$

where F_{ESj} = the number of j th environmental suitability value ($j \leq i$); N = the total number of grid cells in the entire study area.

From a statistical standpoint, P_{in} signifies a discontinuous change in $F(x)$, depicted as a distinct bend or steep turn in the curve as illustrated in Fig. 3. Notably, at P_{in} , there is a marked alteration in the distribution of V_{ES} values, indicating a clear boundary between two sides of V_{ES} values. Hence, the V_{ES} value corresponding to P_{in} is designated as the T_{ES} , demarcating between AFGs and AUGs. The precise position of P_{in} is determined where the second-order derivative of $F(x)$

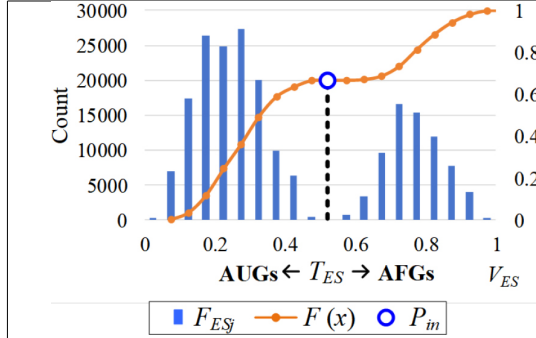


Fig. 3. Demonstration of the cumulative probability distribution curve of environmental suitability values.

279 equals 0, as specified in Eq. (3).

$$f(T_{ES}) = \frac{d^2 F(x)}{dx^2} = 0 \quad (3)$$

280 2.2. Land parcel distribution pattern recognition

281 After deriving the alignment environmental suitability
282 values of each grid cell, AFGs must be clustered into
283 a set of AFRs with various shapes and scales for the
284 subsequent construction of a STM. Spatial clustering
285 approaches play a crucial role in identifying different
286 AFR patches by grouping similar grid cells based on
287 both their environmental suitability values and spatial
288 relative locations into clusters.

289 However, AFRs often have irregular shapes, present-
290 ing challenges in accurately locating and determining
291 their scales. Traditional clustering algorithms, such as
292 the commonly used k-mean clustering algorithm [38],
293 may require a predetermined cluster number and prove
294 ineffective for clustering irregularly shaped groups. To
295 address this challenge, a density-based clustering algo-
296 rithm known as DBSCAN (Density-Based Spatial Clus-
297 tering of Applications with Noise) is employed. DB-
298 SCAN can identify clusters of arbitrary shapes without
299 requiring prior knowledge of the number and centers
300 of clusters [39,40]. In the DBSCAN algorithm, a point
301 is classified as a core point if the number of neighbor-
302 ing points, called seed points, within a specified radius
303 (ϵ) exceeds a certain threshold. This algorithm requires
304 two key parameters: the radius (ϵ) and the minimum
305 number of points (N_{min}). A customized flow of the
306 DBSCAN algorithm for identifying the distribution pat-
307 tern of AFRs is presented below:

308 Step 1: Initialize all grid cells as unclassified and set
309 $T = 1$.

310 Step 2: Starting from the top left and moving to-
311 wards the bottom right, examine each un-
312 classified grid cell to determine if it qualifies
313 as a core point using the parameters ϵ and
314 N_{min} . A grid cell is designated as a core point
315 (G_P) and assigned to cluster C_T if the num-
316 ber of alignment-favorable grid cells within
317 a circle centered at the grid cell with a radius
318 ϵ exceeds the predefined threshold N_{min} . Its
319 seed points (G_S) are recorded accordingly
320 in a set called Ω . Otherwise, proceed to the
321 next grid cell.

322 Step 3: Select G_S from Ω , add it to cluster C_T , mark
323 it as classified, and remove it from Ω .

324 Step 4: Check if G_S qualifies as a core point with
325 the parameters ϵ and N_{min} . If it does, add
326 its unclassified seed points to Ω . If it does
327 not, return to Step 3.

328 Step 5: Repeat Steps 3 and 4 until all grid cells in Ω
329 are classified.

330 Step 6: Increase the value of T by 1 ($T = T + 1$),
331 and repeat Steps 2 to 5 until no more core
332 points remain.

333 Step 7: Assign grid cells that do not belong to any
334 cluster as noise.

335 After implementing the DBSCAN algorithm, the
336 AFRs are grouped into clusters, and each grid cell is as-
337 signed a cluster label (C_T) accordingly. Subsequently,
338 the distribution pattern of AFRs is determined by the
339 relative locations of the clusters with respect to the start
340 and end points. The specific identification formulas are:

$$x_{min} \leq \min(x_S, x_E); x_{max} \geq \max(x_S, x_E) \quad (4)$$

$$y_{min} \leq \min(y_S, y_E); y_{max} \geq \max(y_S, y_E) \quad (5)$$

341 where x_{min} , y_{min} , x_{max} , y_{max} = the minimum and
342 maximum boundaries of each alignment-favorable clus-
343 ter and x_S , y_S , x_E , y_E = the coordinates of the start
344 and end points.

345 If a cluster of AFRs satisfies the criteria stated in
346 both Constraints (2) and (3), the AFRs are continuous
347 throughout the study area (Fig. 3a). However, if none
348 of the alignment-favorable clusters satisfy Constraint
349 (2) but at least one cluster satisfies Constraint (3), the
350 AFRs are concentrated within the study area (Fig. 4b).
351 Otherwise, AFRs' distribution pattern presents an IIEs,
352 as shown in Fig. 4c.

353 The purpose of clustering AFRs is to efficiently gen-
354 erate paths within and between AFRs using specific
355 strategies in the following path development process.
356 However, the shape of AFRs is extremely irregular, and

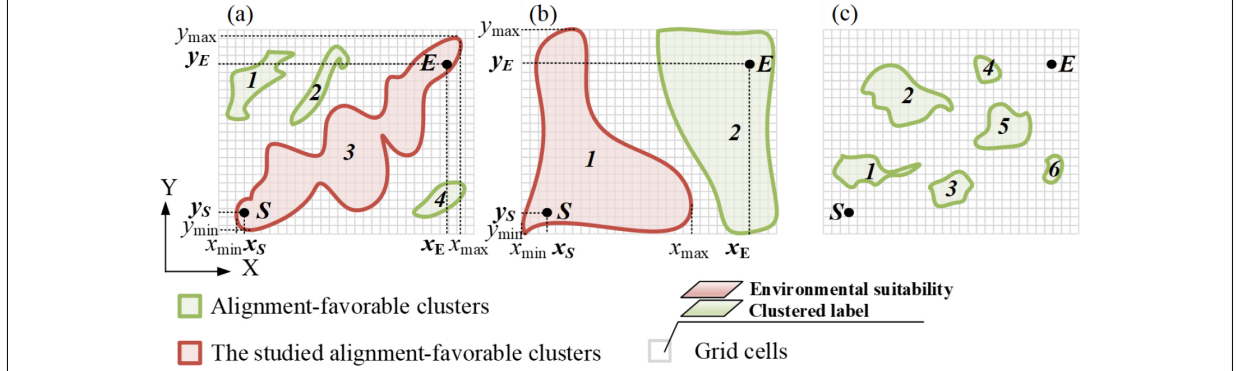


Fig. 4. Alignment-favorable clusters are (a) continuous; (b) obstructed and (c) isolated.

can be generally divided into convex and concave polygons. The complex shape of the convex polygons is very detrimental to efficient connection between them. Therefore, to facilitate subsequent separated path generation procedures, AFRs are unified as convex polygons by identifying and transforming concave polygons into convex polygons [41]. The specific steps are listed as follows:

Step 1. Connect the vertexes (A, A_1, \dots, A_n) of an AFR in a clockwise direction. Then, identify whether the shape of this AFR is a concave polygon with the following formulas:

$$\begin{cases} \overline{A_0 A_1} \times \overline{A_1 A_2} < 0 \\ \overline{A_1 A_2} \times \overline{A_2 A_3} < 0 \\ \dots \\ \overline{A_{n-2} A_{n-1}} \times \overline{A_{n-1} A_n} < 0 \end{cases} \quad (6)$$

where $\overline{A_{n-2} A_{n-1}} \times \overline{A_{n-1} A_n}$ is the vector cross product of the vector at A_{n-2} and A_{n-1} with the vector at A_{n-1} and A_n . If the value of this vector cross product exceeds 0, this polygon is concave at A_{n-1} , as shown in Fig. 5b. Otherwise, this AFR presents a convex shape as shown in Fig. 5a.

Step 2. Extend $\overline{A_{n-2} A_{n-1}}$ in the direction of this vector to split this polygon into two sub-polygons (i.e., P_{P1} and P_{P2} in Fig. 5c).

Step 3. Repeat Steps 1 and 2 to check whether these are convex polygons, until all the sub-polygons are convex.

3. Isolated island effect representation

3.1. Structure of semantic topological map

In this study, the focus is on alignment development in a study area exhibiting an IIE, where each

alignment-favorable cluster is called an island. To effectively utilize the island distribution features and assist the alignment optimization process, a specific data structure is required to represent these features. A semantic topological map (STM), which comprises nodes and edges, can provide an intuitive and easily understandable visualization of the complex system under investigation [42]. Therefore, the island distribution features are abstracted and represented as an STM, denoted as G . The topology structure of this STM can be expressed as:

$$G = (V, P_S, P_E, E_{off}, E_{on}, W_{E_{off}}, W_{E_{on}}) \quad (7)$$

where $V = \{v_1, v_2, \dots, v_n\}$ denotes a set of temporary nodes that store the locations and scales of islands, n is the number of islands; $P_S = \{p_{s1}, p_{s2}, \dots, p_{sn}\}$ and $P_E = \{p_{e1}, p_{e2}, \dots, p_{en}\}$ represent the start and end nodes set for every island; $E_{off} = \{e_{12}, e_{13}, \dots, e_{ij}\}$ indicates a set of off-island edges, where $e_{ij}(v_i, v_j)$ is the off-island edge connecting v_i and v_j (among which, v_i and v_j represent two temporary nodes directly connected, v_i is a former node and v_j is a latter node); $E_{on} = \{e_{on1}, e_{on2}, \dots, e_{oni}\}$ denotes on-island edges, where $e_{oni}(p_{si}, p_{ei})$ is the on-island edges connecting each pair of start and end points of v_i ; $W_{E_{off}}, W_{E_{on}}$ = the alignment suitability costs set for the off-island edges and on-island edges, respectively.

For the STM, a graph adjacent matrix (A_M) is used for describing the adjacency relations between every island pair:

$$A_M = \{a_{ij}\}_{n \times n}$$

$$a_{ij} = \begin{cases} 1, & \text{if } e_{ij}(v_i, v_j) \in E_{off} \\ 0, & \text{if } e_{ij}(v_i, v_j) \notin E_{off} \end{cases} \quad (8)$$

where a_{ij} is the element in the i th row and j th column for A_M , while n is the number of islands. It is noted that $a_{ij} = 1$ means v_i and v_j are adjacent in an STM.

In the STM representing the island distribution features, it is important to consider that an island may have multiple start and end nodes. To capture the connectivity information among these nodes, the connecting conditions of each start and end node pair are stored in on-island edges specific to that particular island. Each edge represents the connection between a start node and an end node, and there can be multiple such connections within the island. Therefore, to fully represent the connectivity within the island, $p \times q$ on-island edges are required for an island with p start nodes and q end nodes.

3.2. Constructing a semantic topological map

The construction of a STM involves two key procedures: between-island connectivity and within-island path determination.

3.2.1. Between-island connectivity

In this procedure, alignment-favorable clusters are treated as temporary nodes, and their adjacency relations are recorded in off-island edges. The temporary nodes are assigned numbers based on the coordinates of their centers of gravity. To assign these numbers, the centers of gravity of all nodes are projected onto an x -axis, and the nodes are numbered sequentially from left to right, starting from 1. If there are multiple nodes with the same x -coordinate, their numbers increase as the y -coordinate increases. After the temporary nodes are numbered (as shown in Fig. 6a), the locations of the off-island edges and their alignment suitability costs are determined using a devised multi-directional scanning process. This scanning process involves systematically scanning the study area with line segments in different directions, as shown in Fig. 7. These scanning line segments, denoted as L , can be expressed as follows:

$$\begin{aligned} L &= Y_2 \cup Y_3 \\ \begin{cases} Y_1 = \frac{Y_E - Y_S}{X_E - X_S} \cdot X + \frac{X_E \cdot Y_S - X_S \cdot Y_E}{X_E - X_S} \\ Y_2 = Y_1 + N \cdot W \\ Y_3 = R(Y_2) \end{cases} & (9) \\ X &\in [X_L, X_R]; \\ N &\in \left[-\frac{Y_U - Y_D}{2 \cdot W}, \dots, 0, 1, \dots, \frac{Y_U - Y_D}{2 \cdot W} \right] \end{aligned}$$

where Y_1 = the base scanning line crossing the start and end points; Y_2 = the translational scanning line set derived by translating Y_1 upwards and downwards at the spacing of the grid cell width; Y_3 = the rotational scanning line set obtained by rotating Y_2 n times (i.e.,

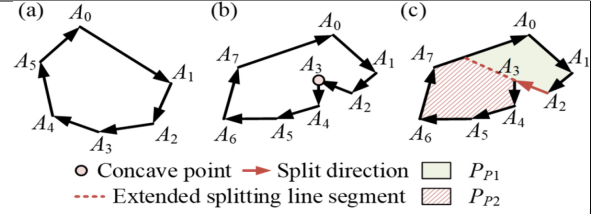


Fig. 5. AFRs in the shape of (a) a convex polygon; (b) concave polygon and (c) division of concave polygon into convex polygons.

36) with rotation angles $5^\circ, 10^\circ, \dots, 180^\circ$; X, Y = the design variables of L , representing the coordinates of the points located on the scanning lines; X_L, X_R = the left and right boundaries of X ; Y_U, Y_D = the upper and lower boundaries of Y ; N = the number of translational lines; W = the width of a grid cell and R = the rotation transformation of a line, whose rotation angle (α) ranges from 0° to 180° at 5° intervals in this study.

By implementing this multi-directional scanning strategy, the optimized connection between any two AFRs islands can be derived with the following procedures:

Step 1. Determine the former and latter nodes:

Intercept the line segments connecting islands v_i and v_j from the previously mentioned set of multi-directional scanning lines (L). Define the endpoints of these line segments located on island v_i (or v_j) as P_{ei} (or P_{sj}).

Compute the distances of P_{ei} and P_{sj} from the start point.

If P_{ei} is closer to the start point, it is designated as the former node.

P_{ej} is defined as the latter node.

Step 2. Record the directed line segments:

The directed line segments connecting v_i and v_j is recorded in the line segments set Φ_{ij} .

Step 3. Compute the environmental suitability cost

(C_L) of line segments in Φ_{ij} . Specifically, C_L is computed by accumulating the difference between the maximum V_{ES} (V_{ESmax}) in the study area and the V_{ES} value of every grid cell traversed by this line segment. Assuming that the line segment traverses N grid cells the environmental suitability cost, C_L is computed as:

$$C_L = \sum_{k=1}^N (V_{ESmax} - V_{ESk}) \quad (10)$$

Afterward, the line segment with the minimum C_L value is designated as the edge (e_{ij}) between v_i and v_j .

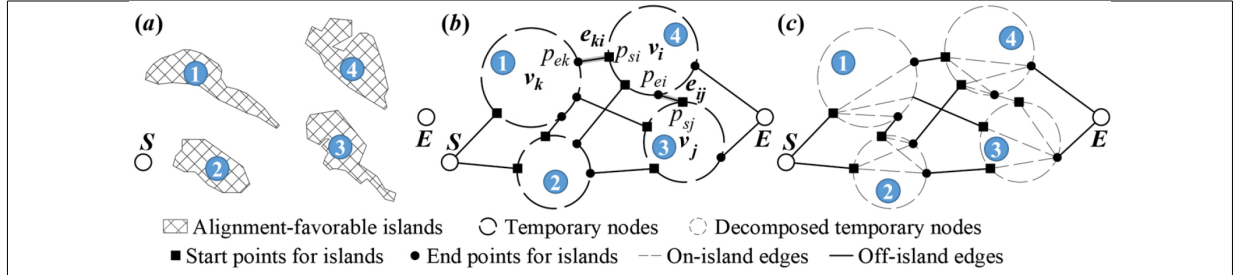


Fig. 6. (a) The AFRs distribution in a study area with an IIE; (b) temporary nodes decomposition and (c) the final topology structure of the STM.

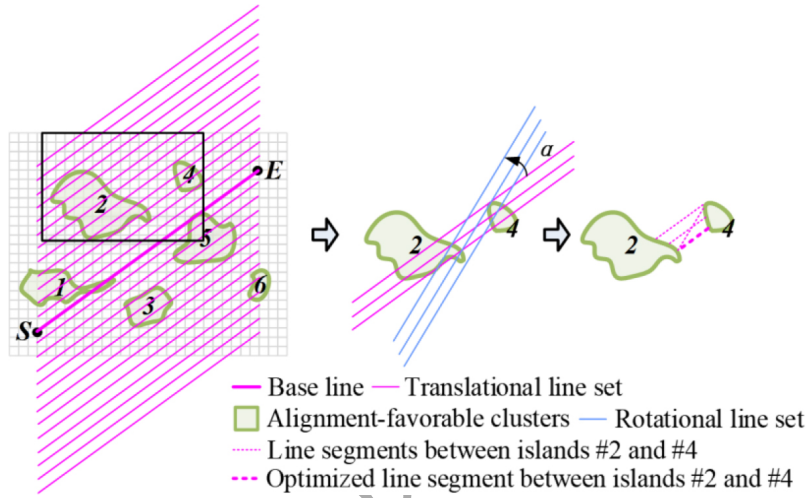


Fig. 7. Scanning lines and the line segments between two alignment-favorable regions (i.e., temporary nodes).

Then, a_{ij} of e_{ij} is assigned as 1, and W_{Eoff} for e_{ij} is:

$$W_{Eoff}(e_{ij}) = \min C_L(x_i, y_i, x_j, y_j) \quad (11)$$

where x_i, y_i, x_j, y_j , are the coordinates of two endpoints (p_{ei}, p_{sj}) of the line segment with the minimum environmental suitability cost. These endpoints are stored in the variable e_{ij} , which provides the start and end points for generating subsequent paths within each temporary node. It is important to note that for an edge e_{ij} , p_{ei} represents an endpoint of v_i , while p_{sj} represents a start point of v_j , as shown in Fig. 6b.

3.2.2. Within-island path determination

To generate paths within a temporary node (v_i) that has multiple start and end points, the node is further decomposed based on these points. Each start and end point is treated as a separate node, and all pairs of start and end points are connected to determine the on-island edges. The weight of each on-island edge (W_{oni}) is assigned as the minimum accumulating environmental suitability cost of the paths between the corresponding endpoints. Handling multiple start and end points within

a temporary node can be viewed as a Multi-Source Shortest-Path (MSSP) problem. The Floyd-Warshall algorithm [43] is a typical MSSP algorithm that can find the shortest paths between all pairs of nodes in a graph. It is both intuitive and easy to implement. Thus, it is used in this work for efficiently determining the optimized paths. To apply the Floyd-Warshall algorithm to the optimization of on-island paths, two adaptations are made, addressing the study area and the traditional Floyd-Warshall algorithm separately.

1. Regarding the study area, a sub-graph representing the study area within each temporary node is constructed. Using a circular-shaped window mask, as proposed by Song et al. [3], every grid cell within the temporary node is scanned. Grid cells satisfying the design constraints, including the center grid cell and its boundary grid cells, are designated as nodes in the sub-graph. The lines connecting the center grid cell with the boundary grid cells are considered as edges in the sub-graph.

2. Simultaneously, the Floyd-Warshall algorithm is parallelized for the optimization of on-island paths within each node. In more detail, during the between-island paths determination procedure, the start and end points of each node are obtained and designated as the input for the Floyd-Warshall algorithm. Consequently, all optimized within-island paths can be derived through a single loop of the Floyd-Warshall algorithm, eliminating the need to sequentially traverse every node.

Afterward, the Floyd-Warshall algorithm is applied to each sub-graph until the costs from the start points to the end points are stabilized, ensuring the optimized paths are determined.

By following these procedures, an STM is generated (as shown in Fig. 6c), representing the distribution characteristics of islands. Additionally, environmental suitability costs are assigned to each node and edge within the map, providing valuable information for further alignment search processes.

4. Alignment optimization method

4.1. Alignment search process

In the alignment optimization process, the STM with determined edge suitability is used. Dijkstra's algorithm, known for its effectiveness in path optimization problems, has been successfully applied in various contexts, including alignment optimization [3,44]. It is also employed in this paper. Dijkstra's algorithm, as applied to alignment optimization, is outlined below:

Step 1: Add all the nodes in the STM to a node set, N_S .

Step 2: Designate two arrays for each node: one for storing the environmental suitability cost ($\text{dis}[v]$), and another for storing its former adjacent node in the optimized path from the start point ($\text{for}[v]$). Initialize $\text{dis}[v]$ as infinity for all nodes, except for the start point which is assigned a value of 0. The former adjacent node for the start point is itself, while the values in $\text{for}[v]$ for other nodes are undefined.

Step 3: Choose the node, v_i , with the minimum $\text{dis}[v_i]$ value from N_S and remove it from N_S . Find all the latter adjacent nodes (V_L) of v_i from N_S . Latter adjacent nodes refer to nodes that are farther from the start point than v_i , as stated in Section 3.2 of the paper.

Step 4: Compute the environmental suitability cost ($W_E(e_{ij})$) from a latter adjacent node (v_j) to v_i . If $\text{dis}[v_i] + W_E(e_{ij})$ is less than the current $\text{dis}[v_j]$ value, update $\text{dis}[v_j]$ as $\text{dis}[v_i] + W_E(e_{ij})$ and set $\text{for}[v_j]$ as v_i .

Step 5: Repeat Step 4 until the $\text{dis}[v]$ and $\text{for}[v]$ values of all the latter adjacent nodes have been updated.

Step 6: Repeat Steps 3 to 5 until there are no elements left in N_S .

By following these steps, Dijkstra's algorithm computes the distance (environmental suitability cost) from each node to the start point, while also storing the predecessor (former adjacent node) in the optimized path. This process continues until all nodes have been visited and processed, resulting in an optimized alignment that considers environmental suitability costs between nodes. Specifically, an optimized path development process between an observed node and the start point is shown in Fig. 8.

4.2. Constraints

In the process of generating a railway alignment, it is necessary to consider multiple constraints related to geometric, structural, and locational aspects. These constraints ensure that the alignment satisfies the necessary design criteria and construction limitations, while avoiding sensitive or forbidden regions.

- (1) The geometric constraints focus on ensuring that the alignment profile adheres to the specific design criteria for railways. These criteria may include considerations such as vertical and horizontal clearances, minimum curve radius (R_{min}), and maximum gradient.
- (2) Structural constraints take into account the limitations of the available construction techniques. They consider factors such as the type of terrain, soil conditions, and construction equipment capability. These constraints ensure that the alignment can be constructed safely and efficiently.
- (3) Locational constraints primarily revolve around avoiding environmentally sensitive areas and forbidden regions. This includes areas with protected flora and fauna, cultural heritage sites, residential areas, and other designated areas that should be avoided due to legal or social reasons.

As outlined in Section 1, the primary contribution of the proposed method lies in generating an optimized alignment corridor during the area-corridor stage, in-

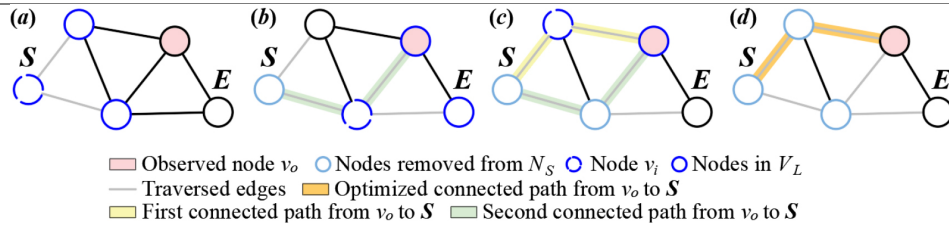


Fig. 8. Path generation process of Dijkstra's algorithm.

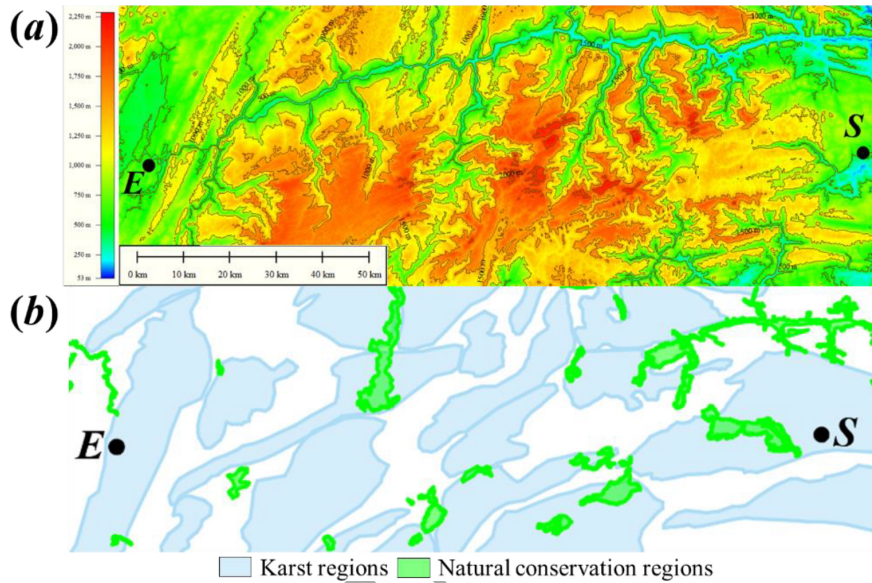


Fig. 9. (a) The terrain and (b) the geology maps of the study area.

629 tended to provide an initial alternative for the subse-
 630 quent corridor-alignment optimization stage.

631 The corridor-alignment optimization typically in-
 632 volves two steps:

633 Step 1: The initial output, representing the opti-
 634 mized path solution from the proposed
 635 method, is subjected to a fitting process. This
 636 process involves configuring curves with a
 637 minimum allowable radius (R_{min}) to points
 638 of intersection (PIs) along the optimized
 639 path. Detailed procedures, as described in
 640 Li et al. [45], are followed to check the
 641 corresponding minimum allowable tangent
 642 lengths.

643 Step 2: To ensure alignment re-optimization after
 644 deviations from the initial optimized path,
 645 nature-inspired optimization methods such
 646 as genetic algorithms (GA) and particle
 647 swarm optimization (PSO) are employed.
 648 These methods iteratively adjust the loca-
 649 tions of PIs within a specific corridor, de-

650 fined by the optimized path as the centerline
 651 and a designated width as a buffer zone. The
 652 adjustment process continues until the objec-
 653 tive function of the alignment optimization
 654 converges to an optimized value.

655 It is noted that the generated alignment alternatives
 656 must adhere to the aforementioned alignment design
 657 constraints.

658 5. Case study

659 5.1. Case profile

660 In this study, the focus is on the W-E High-Speed
 661 Railway (HSR), which is a railway under construction.
 662 The railway has a maximum design speed of 350 km/h
 663 and spans a distance of 153 km. It is located in the
 664 southwest region of Hubei Province, where there is a
 665 significant presence of karst landforms in the undulating
 666 mountainous areas [46]. Karst landforms are formed

Table 1
Unit costs

Item	Value	Item	Value
Rail track (10^4 ¥/m)	0.46	Right-of-way (¥/m ²)	13.4
Fill earthwork (¥/m ³)	65	Cut earthwork (¥/m ³)	32
(100 m < h < 150 m) Bridge (10^4 ¥/m)	15	(h < 100 m) Bridge (10^4 ¥/m)	14
(L < 1 km) Tunnel (10^4 ¥/m)	11.5	(1 km < L < 4 km) Tunnel (10^4 ¥/m)	10.5
(L > 4 km) Tunnel (10^4 ¥/m)	13.5	One bridge abutment/tunnel portal (10^4 ¥)	20

due to the long-term effects of groundwater and surface water on soluble rocks, resulting in unique features such as gullies, funnels, and caves. These landforms pose potential risks to railway alignments, particularly in tunnel sections [47,48]. Karst geological disasters like collapses, water invasion, and mud gushing can severely impact tunnel construction, causing damage to equipment and even casualties [49,50]. The YiChang-Wanzhou railway, which is a section of the HSR in this study area, has already been constructed and faced significant challenges in dealing with karst hazards along its route [49]. Therefore, it is desirable to completely bypass karst landforms when planning the alignment for the W-E HSR. However, when the railway is situated in a mountainous region with undulating terrain and dense karst landforms, it becomes highly likely that the alignment will encounter karst areas. In such situations, it is important to ensure that there is sufficient clearance between the alignment and karst regions, satisfying the required safety standards, considering topologic and geologic conditions. Moreover, the study area also includes multiple natural conservation areas, which must be traversed using bridges or tunnels in order to minimize environmental impact. In total, there are 19 karst regions and 14 natural conservation areas within the study area, covering a significant fraction of the terrain. Terrain and geology maps for the study area, as well as unit costs for railway construction, are obtained from the China Railway Siyuan Survey and Design Group Co. Ltd., as demonstrated in Fig. 9 and Table 1, respectively.

It is notable that the terrain in this area is characterized by significant undulations, with a maximum elevation difference of 2,197m. Therefore, the maximum allowable gradient (G_{\max}) for the railway is set at 30‰ taking into account the steepness of slopes. Considering the topography in optimizing the design, it is advisable to create vertical alignments that follow the natural undulations of the terrain. This approach helps to reduce tunnel lengths and control bridge heights, thus minimizing construction costs and potential environmental impacts. The karst landforms are densely distributed throughout the entire study area, leaving only narrow

and irregular non-karst areas. Thus, the railway alignment is highly likely to encounter karst regions along its route. Given the potential risks associated with karst hazards, it is essential to plan the alignment carefully in order to avoid or mitigate these challenges. Bypassing karst areas entirely and ensuring a sufficient clearance between the alignment and the karst regions should be a priority for ensuring the safety and stability of the railway construction.

5.2. Results

5.2.1. Land parcel treatment

(1) Environmental suitability distribution

The environmental suitability map of the study area is generated using Eq. (1) and presented in Fig. 10a. Subsequently, the cumulative probability distribution curve, as illustrated in Fig. 11, is obtained for all environmental suitability (V_{ES}) values by applying the second derivative to Eq. (2). The threshold V_{ES} value (T_{ES}) demarcating AFRs and AURs is then computed using Eq. (3), and in this case, the threshold value is set at 0.5.

In this regard, the grid cells with a V_{ES} value exceeding T_{ES} are identified as AFRs for the railway. It is observed that approximately 33.4% of the study area consists of AFRs, but most of them are isolated and surrounded by AURs.

(2) Alignment-favorable regions clustering

The radius (ϵ) and the minimum number of points (N_{\min}) are two crucial parameters in the DBSCAN algorithm, significantly influencing the scales and number of clusters. In this scenario, opting for a smaller ϵ is preferred to prevent different obstacles from being clustered into the same group. Accordingly, ϵ is set as the minimum distance between two obstacles, and the value of N_{\min} is set to 90% of the result obtained by dividing the area of a circle with ϵ as the radius by the area of the grid cell. Once these key parameters are established, the DBSCAN clustering algorithm is applied to identify distinct AFRs. This algorithm accurately pinpoints the locations and scales of these regions, referred to as islands in this study. In the present case, 13 islands are identified, as depicted in Fig. 10b.

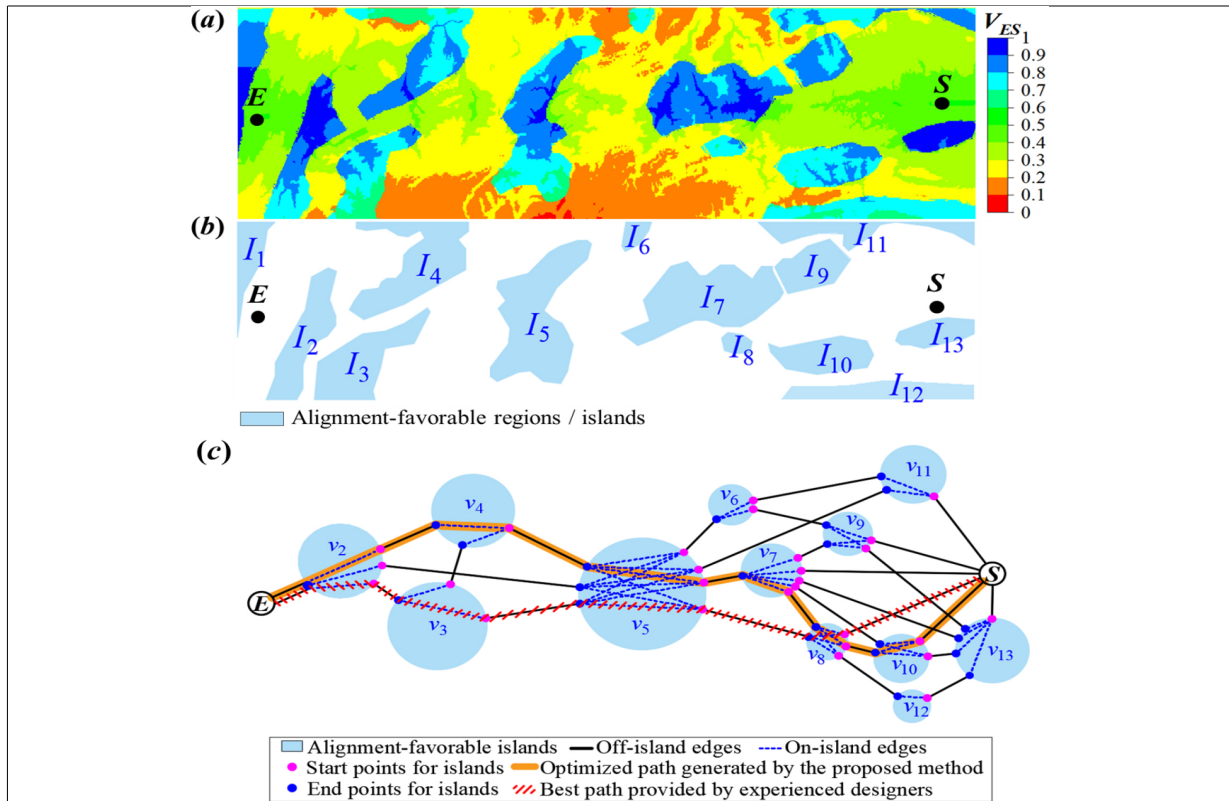


Fig. 10. (a) Environmental suitability map for alignments; (b) the distribution of AFRs; (c) semantic topological map of the study area.

752 (3) Construction of semantic topological map

753 Through the specific multi-directional scanning process and the implementation of the Floyd-Warshall algorithm, a STM is constructed, including the sequential generation of between-island and within-island paths, as shown in Fig. 10c.

758 5.2.2. Alignment solutions

759 Following the construction of the STM, an alignment optimization process is carried out based on this map. It turns out that the path optimized in this process traverses islands 10, 8, 7, 5, 4, and 2, as determined by the proposed method. In comparison, the alignment provided by human designers traverses islands 8, 5, 3, and 2. It is noteworthy that the proposed method selects additional islands (10, 7, and 4) that were not considered in the human-designed alignment. This result highlights that the constructed STM offers diverse alignment alternatives for railway design. The proposed method provides an expanded range of options by considering additional islands, thereby allowing for a more comprehensive exploration of possible alignments.

773 Subsequently, the optimized path is fitted using the method described in Section 4.2, and the derived initial

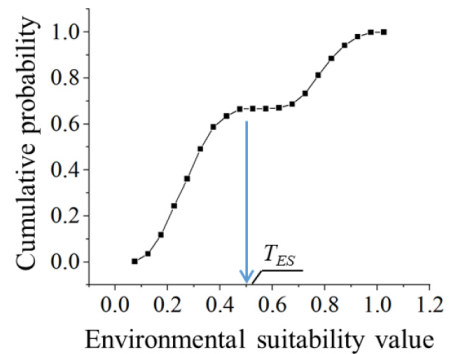
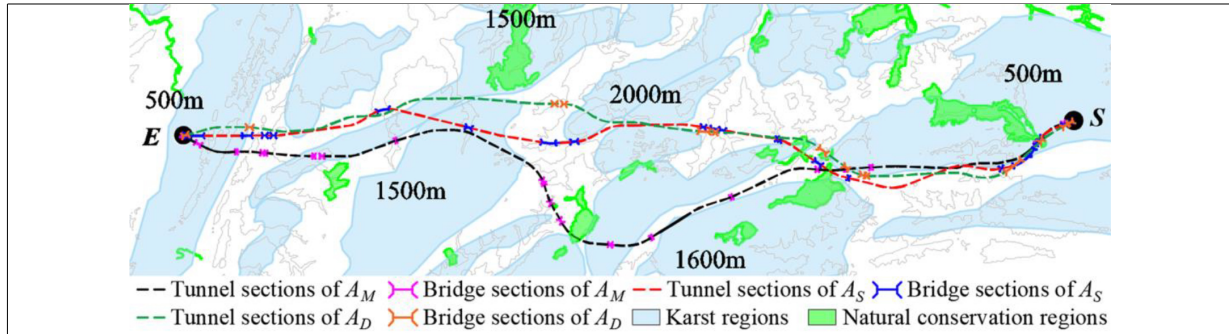
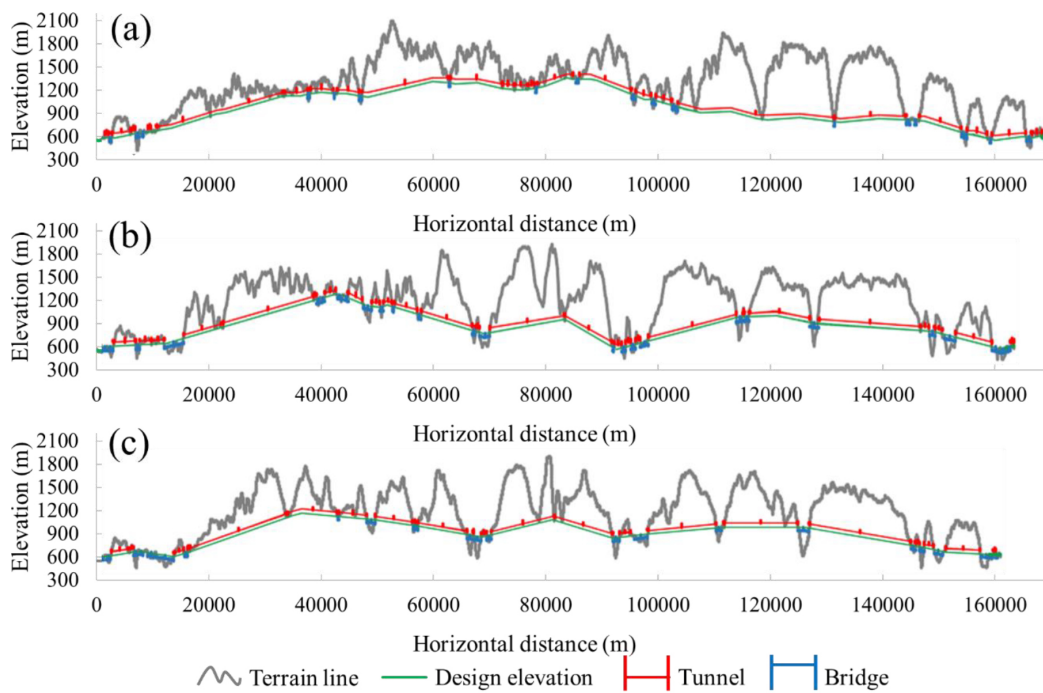


Fig. 11. Cumulative probability distribution curve of V_{ES} values.

775 alignment alternative serves as input to a previously established PSO method [23] for generating the detailed alignment solution.

776
777
778 In this paper, a previous environmental suitability analysis-assisted 3D-DT (ES-3D-DT) algorithm from Pu et al. [34] is taken as a benchmark method to showcase the effectiveness of the proposed method in solving alignment optimization problems within study areas characterized by densely-distributed obstacles.

783
784 In the ES-3D-DT method, the study area is repre-

Fig. 12. Horizontal alignments of A_M , A_D and A_S .Fig. 13. Vertical alignments of (a) A_M (b) A_D and (c) A_S .

785 sented as a set of voxels, and the V_{ES} values for all fea-
 786 sible voxels is computed using Eq. (1). Subsequently,
 787 environmental suitability grades (Grade I, II, and III)
 788 are assigned based on the derived V_{ES} . During the align-
 789 ment search, voxels with Grade III environmental suit-
 790 ability, indicating unfavorable for alignments, are ex-
 791 cluded from consideration. The detailed flow chart of
 792 the ES-3D-DT method can be found in Pu et al. [34].

793 Both the ES-3D-DT and the proposed method are
 794 executed on a computer with Intel Core i7-7700 CPU
 795 @ 3.60 GHz, with the grid resolution of the study area
 796 set at 30 m. The ES-3D-DT method requires 135 min-
 797 utes to produce the optimized alignment corridor. In
 798 contrast, the proposed method leverages Dijkstra's al-

799 gorithm to generate the optimized path based on the de-
 800 rived STM within a significantly reduced time frame of
 801 113 seconds. Considering that the time to construct the
 802 STM is 621 seconds for this case, the proposed method
 803 notably enhances the efficiency of the alignment corri-
 804 dor optimization process. Afterward, the best corridors
 805 derived from both ES-3D-DT and the proposed method
 806 are refined with the customized PSO for obtaining the
 807 detailed alignment solutions, designated as A_D and
 808 A_S , derived from the corridors created by ES-3D-DT
 809 and the proposed method, respectively. A_D and A_S
 810 are further compared with the best alignment (A_M) pro-
 811 vided by experienced designers from the China Railway
 812 Siyuan Survey and Design Group Co. Ltd. Their hori-

Table 2
Numerical comparisons of A_M , A_D and A_S

Item	A_M	A_D	A_S
Railway length (m)	168,739	163,311	160,974
Right-of-way area (m ²)	357,903	347,691	352,962
Filling/Cutting volume (m ³)	24,949/151,751	25,638/163,522	25,093/161,305
Number of bridges (100 m < h < 150 m)-Total length (m)	25-19,573	22-20,219	14-11,852
Number of bridges (h < 100 m)-Total length (m)	3-2,461	4-5,873	10-13,159
Total number-length of bridges (m)	28-22,034	26-26,092	24-25,011
Number of tunnels (L < 1 km)-Total length (m)	13-7,396	6-3,819	8-3,449
Number of tunnels (1 km < L < 4 km)-Total length (m)	15-35,265	10-19,930	4-8,481
Number of tunnels (L > 4 km)-Total length (m)	10-103,881	10-109,047	11-117,729
Total number-length of tunnels (m)	38-146,542	26-132,796	23-129,659
Total bridge length in karst regions (m)	8,909	6,530	10,685
Total tunnel length in karst regions (m)	75,628	54,960	42,899
Total alignment length in karst regions (m)	84,537	61,490	53,584
Total alignment length in natural conservation regions (m)	3,386	2,355	3,135
Total construction cost (million ¥)	22,530	21,780	21,618
Improvement	N/A	3.3%	4.0%
Alignment suitability cost	2,690	2,548	2,415
Improvement	N/A	5.3%	10.2%

zontal and vertical alignments are shown in Figs 12–13, and detailed comparison data are provided in Table 2.

Based on the observations and comparisons, several key findings can be highlighted:

- (1) Both A_D and A_S result in shorter railways (i.e., 5,428m and 7,765m for A_D and A_S , respectively) compared to A_M . These reductions contribute to a smoother geometric profile of the HSR, which is advantageous for subsequent railway operation and maintenance stages.
- (2) In comparison with A_M , the total tunnel lengths decreased significantly by 13,746m and 16,883m, while the total bridge lengths increased slightly by 4,058m and 2,977m for A_D and A_S , respectively. By shortening the expensive tunnels, the construction costs for A_D and A_S are reduced by 3.3% and 4.0%, respectively.
- (3) In terms of the karst hazard avoidance, A_D decreases the length of alignment sections that traverse karst hazard regions, including shortening most karst-sensitive tunnels compared to A_M . A_S performs even better than A_D by further reducing alignment and tunnel lengths in karst regions.
- (4) Concerning natural conservation regions, A_D exhibits the best performance by reducing the length of alignment traversing sections to 2,355m compared to A_M 's 3,386m. It can be found that A_D effectively bypasses sparsely-distributed natural conservation regions, but struggles with densely-distributed karst regions compared to A_S . Therefore, A_S achieves the best performance, improving alignment environmental suitability cost by 10.2% compared to A_M .

In summary, the analyses demonstrate that the proposed model and method (A_S) outperform both the optimized alignment (A_D) generated by the ES-3D-DT and the manually-designed alignment (A_M) in terms of reduced karst coverage, lower construction cost, and improved environmental suitability. A_S effectively optimizes the alignment by minimizing tunnel lengths and overall railway footprint. These findings highlight the potential value of using the proposed model and method to generate alignment alternatives that offer both cost efficiency and environmental benefits.

6. Conclusion

In the context of highly-constrained study areas, where alignment-favorable regions (AFRs) are isolated and alignment design is a challenging task, a novel approach is proposed here for addressing this problem. In this approach, environmental suitability analysis is employed to identify AFRs, while an STM is used to depict the distribution pattern of these AFRs. Through this process, the complicated alignment optimization problem is simplified into a shortest path problem, which can be effectively solved using conventional shortest path algorithms. The application of the proposed method in a realistic railway case has demonstrated several key findings:

- (1) The method significantly enhances the efficiency of generating optimized alignment corridors within a densely-distributed karst alignment search space. Despite requiring several minutes (i.e., 621s) for land parcel treatment, the sub-

sequent search process only takes 113 seconds, marking a substantial improvement compared to the 135 minutes needed for the ES-3D-DT method.

- (2) Comparisons of alignment solutions highlight the effectiveness of the ES-3D-DT-generated alignment (A_D) in outperforming the best manually designed alignment (A_M). A_D notably reduces construction and environmental suitability costs by 3.3% and 5.3%, respectively, underscoring the significance of environmental suitability analysis in ensuring the quality of alignments derived from computer-aided optimization methods. Moreover, the best alignment (A_S) generated by the proposed method surpasses A_D 's performance. A_S achieves a reduction of 4.0% in construction costs and an improvement of 10.2% in environmental suitability costs compared to A_M .

It is noted that the paper specifically focuses on a study area featuring multiple karst regions as an illustrative example. However, the proposed method is adaptable and applicable to all alignment search spaces characterized by IIEs.

Above all, the proposed method is effective in alignment optimization in a study area with densely-distributed obstacles in terms of computational efficiency and solution quality.

The limitations of this work include the following:

- (1) In this paper, the threshold value of AFRs and RURs is set to the environmental suitability value corresponding to the inflection point of the cumulative probability distribution curve (which is a representation of distribution features of all the environmental suitability values across the study area). However, it becomes necessary to dynamically adjust this threshold value to ensure the aggregation of AFR patches, thereby expanding the applicability of the proposed method across a wider range of study areas. This issue warrants dedicated and specific studies, which the authors intend to undertake in their future research endeavors.
- (2) Some existing methods are adopted in this work, such as the DBSCAN clustering algorithm as well as the Floyd-Warshall Dijkstra's and PSO algorithms. It is important to highlight that these methods form part of a novel alignment optimization framework introduced in this paper. This framework involves three sequential steps: land parcel preprocessing, STM construction,

and optimized path generation based on the derived STM. While these methods are integral to this framework, alternative approaches can be substituted that achieve similar functionalities. For example, other nature-inspired optimization methods such as a neural dynamic model [51], a harmony search algorithm [52], a simulated annealing [53] and a spider monkey optimization method [54] can also be explored for further confirming the effectiveness of the proposed optimization framework.

- (3) Besides, other factors that affect railway alignment design, such as ecologic impacts and social influence, should also be specially-studied and integrated into the alignment traversing suitability analyses.

Acknowledgments

This work is partially funded by the National Key R&D Program of China with award number 2021YFB2600403; National Science Foundation of China: 52078497; Science and Technology Research and Development Program Project of China railway group limited (2022-Major-20); the Fundamental Research Funds for the Central Universities of Central South University (2023ZZTS0378).

References

- [1] Vázquez-Méndez ME, Casal G, Castro A, Santamarina D. An algorithm for random generation of admissible horizontal alignments for optimum layout design. *Computer-Aided Civil and Infrastructure Engineering*. 2021; 36(8): 1056-72. doi: 10.1111/mice.12682.
- [2] Shi J, Zhang Y, Chen Y, Wang Y. A smoothness optimization method for horizontal alignment considering ballasted track maintenance. *Computer-Aided Civil and Infrastructure Engineering*. 2023; 38(6): 739-61. doi: 10.1111/mice.12884.
- [3] Song T, Pu H, Schonfeld P, Liang Z, Zhang M, Hu J, et al. Mountain railway alignment optimization integrating layouts of large-scale auxiliary construction projects. *Computer-Aided Civil and Infrastructure Engineering*. 2023; 38(4): 433-53. doi: 10.1111/mice.12839.
- [4] Song T, Pu H, Schonfeld P, Zhang H, Li W, Hu J. Simultaneous optimization of 3D alignments and station locations for dedicated high-speed railways. *Computer-Aided Civil and Infrastructure Engineering*. 2021; 37(4): 405-26. doi: 10.1111/mice.12739.
- [5] Hirpa D, Hare W, Yves Lucet, Yasha Pushak, Tesfamariam S. A bi-objective optimization framework for three-dimensional road alignment design. *Transportation Research Part C-Emerging Technologies*. 2016; 65: 61-78. doi: 10.1016/j.trc.2016.01.016.
- [6] Zhang H, Song T, Schonfeld P, Pu H, Li W, Hu J, et al. Vertical alignment optimization of mountain railways with terrain-

- driven greedy algorithm improved by Monte Carlo tree search. *Computer-Aided Civil and Infrastructure Engineering*. 2023; 38(7): 873-91. doi: 10.1111/mice.12923.
- [7] Song T, Pu H, Schonfeld P, Zhang H, Li W, Hu J, et al. Mountain railway alignment optimization considering geological impacts: A cost-hazard bi-objective model. *Computer-Aided Civil and Infrastructure Engineering*. 2020; 35(12): 1365-86. doi: 10.1111/mice.12571.
- [8] Karlson M, Karlsson CSJ, Mörtberg U, Olofsson B, Balfors B. Design and evaluation of railway corridors based on spatial ecological and geological criteria. *Transportation Research Part D: Transport and Environment*. 2016; 46: 207-28. doi: 10.1016/j.trd.2016.03.012.
- [9] Zhu Z, Xiao J, Li JQ, Wang F, Zhang Q. Global path planning of wheeled robots using multi-objective memetic algorithms. *Integrated Computer-Aided Engineering*. 2015; 22(4): 387-404. doi: 10.3233/ica-150498.
- [10] Jong JC, Jha MK, Schonfeld P. Preliminary highway design with genetic algorithms and geographic information systems. *Computer-Aided Civil and Infrastructure Engineering*. 2000; 15(4): 261-71. doi: 10.1111/0885-9507.00190.
- [11] Song T, Schonfeld P, Pu H. A review of alignment optimization research for roads, railways and rail transit lines. *IEEE Transactions on Intelligent Transportation Systems*. 2023; 24(5): 4738-57. doi: 10.1109/tits.2023.3235685.
- [12] Maji A, Jha MK. Multi-objective highway alignment optimization using a genetic algorithm. *Journal of Advanced Transportation*. 2009; 43(4): 481-504. doi: 10.1002/atr.5670430405.
- [13] Zhang T, Gao Y, Gao T, Schonfeld P, Wu Y, Zhu Y, et al. A sequential exploration algorithm for the design optimization of horizontal road alignment. *Computer-Aided Civil and Infrastructure Engineering*. 2023; 38(15): 2049-71. doi: 10.1111/mice.12990.
- [14] Gao T, Li Z, Gao Y, Schonfeld P, Feng X, Wang Q, et al. A deep reinforcement learning approach to mountain railway alignment optimization. *Computer-Aided Civil and Infrastructure Engineering*. 2021; 37(1): 73-92. doi: 10.1111/mice.12694.
- [15] Pushak Y, Hare WL, Lucet Y. Multiple-path selection for new highway alignments using discrete algorithms. *European Journal of Operational Research*. 2016; 248(2): 415-27. doi: 10.1016/j.ejor.2015.07.039.
- [16] Jong JC, Schonfeld P. An evolutionary model for simultaneously optimizing three-dimensional highway alignments. *Transportation Research Part B: Methodological*. 2003; 37(2): 107-28. doi: 10.1016/s0191-2615(01)00047-9.
- [17] Babapour R, Naghdi R, Ghajar I, Mortazavi Z. Forest road profile optimization using meta-heuristic techniques. *Applied Soft Computing*. 2018; 64: 126-37. doi: 10.1016/j.asoc.2017.12.015.
- [18] Shafahi Y, Bagherian M. A customized particle swarm method to solve highway alignment optimization problem. *Computer-Aided Civil and Infrastructure Engineering*. 2012; 28(1): 52-67. doi: 10.1111/j.1467-8667.2012.00769.x.
- [19] Ma Z, Chen J. Adaptive path planning method for UAVs in complex environments. *International Journal of Applied Earth Observation and Geoinformation*. 2022; 115: 103133. doi: 10.1016/j.jag.2022.103133.
- [20] Roy S, Maji A. Sampling-based modified ant colony optimization method for high-speed rail alignment development. *Computer-Aided Civil and Infrastructure Engineering*. 2022; 37(11): 1417-33. doi: 10.1111/mice.12809.
- [21] Sushma MB, Roy S, Maji A. Exploring and exploiting ant colony optimization algorithm for vertical highway alignment development. *Computer-Aided Civil and Infrastructure Engineering*. 2022; 37(12). doi: 10.1111/mice.12814.
- [22] Lee ZJ, Su SF, Chuang CC, Liu KH. Genetic algorithm with ant colony optimization (GA-ACO) for multiple sequence alignment. *Applied Soft Computing*. 2008; 8(1): 55-78. doi: 10.1016/j.asoc.2006.10.012.
- [23] Pu H, Song T, Schonfeld P, Li W, Zhang H, Hu J, et al. Mountain railway alignment optimization using stepwise & hybrid particle swarm optimization incorporating genetic operators. *Applied Soft Computing*. 2019; 78: 41-57. doi: 10.1016/j.asoc.2019.01.051.
- [24] de Smith MJ. Determination of gradient and curvature constrained optimal paths. *Computer-Aided Civil and Infrastructure Engineering*. 2006; 21(1): 24-38. doi: 10.1111/j.1467-8667.2005.00414.x.
- [25] Li W, Pu H, Schonfeld P, Yang J, Zhang H, Wang L, et al. Mountain railway alignment optimization with bidirectional distance transform and genetic algorithm. *Computer-Aided Civil and Infrastructure Engineering*. 2017; 32(8): 691-709. doi: 10.1111/mice.12280.
- [26] Deng Y, Chen Y, Zhang Y, Mahadevan S. Fuzzy Dijkstra algorithm for shortest path problem under uncertain environment. *Applied Soft Computing*. 2012; 12(3): 1231-7. doi: 10.1016/j.asoc.2011.11.011.
- [27] Lee J, Yang J. A fast and scalable re-routing algorithm based on shortest path and genetic algorithms. *International Journal of Computers Communications & Control*. 2014; 7(3): 482. doi: 10.15837/ijccc.2012.3.1389.
- [28] Sushma MB, Maji A. A modified motion planning algorithm for horizontal highway alignment development. *Computer-Aided Civil and Infrastructure Engineering*. 2020; 35(8): 818-31. doi: 10.1111/mice.12534.
- [29] Yang D, He Q, Yi S. Underground metro interstation horizontal-alignment optimization with an augmented rapidly exploring random-tree connect algorithm. *Journal of Transportation Engineering Part A Systems*. 2020; 146(11). doi: 10.1061/jtepbs.0000454.
- [30] Mondal S, Lucet Y, Hare W. Optimizing horizontal alignment of roads in a specified corridor. *Computers & Operations Research*. 2015; 64: 130-8. doi: 10.1016/j.cor.2015.05.018.
- [31] Pu H, Wan X, Song T, Schonfeld P, Peng L. A 3D-RRT-star algorithm for optimizing constrained mountain railway alignments. *Engineering Applications of Artificial Intelligence*. 2024; 130: 107770-0. doi: 10.1016/j.engappai.2023.107770.
- [32] Li J, Deng G, Luo C, Lin Q, Yan Q, Ming Z. A hybrid path planning method in Unmanned Air/Ground Vehicle (UAV/UGV) cooperative systems. *IEEE Transactions on Vehicular Technology*. 2016; 65(12): 9585-96. doi: 10.1109/tvt.2016.2623666.
- [33] Hu J, Hu Y, Lu C, Gong J, Chen H. Integrated path planning for unmanned differential steering vehicles in off-road environment with 3D terrains and obstacles. *IEEE Transactions on Intelligent Transportation Systems*. 2021; 23(6): 1-11. doi: 10.1109/tits.2021.3054921.
- [34] Pu H, Wan X, Song T, Schonfeld P, Li W, Hu J. A geographic information model for 3-D environmental suitability analysis in railway alignment optimization. *Integrated Computer-aided Engineering*. 2023; 30(1): 67-88. doi: 10.3233/ica-220692.
- [35] Wan X, Pu H, Schonfeld P, Song T, Li W, Peng L, et al. Mountain railway alignment optimization based on landform recognition and presetting of dominating structures. *Computer-Aided Civil and Infrastructure Engineering*. 2023; 39: 242-63. doi: 10.1111/mice.13073.
- [36] Code for design of railway line. China Ministry of Railways,

- 1107 TB 10098-2017; 2017. 1143
- 1108 [37] Quality requirement for digital surveying and mapping 1144
- 1109 achievements. Beijing: Standardization Administration of
- 1110 China; 2008. [47] Alija S, Torrijo FJ, Quinta-Ferreira M. Geological engineer-
- 1111 [38] Ismkhan H. I-k-means+: An iterative clustering algorithm 1145
- 1112 based on an enhanced version of the k-means. Pattern Recog- 1146
- 1113 nition. 2018; 79: 402-13. doi: 10.1016/j.patcog.2018.02.015. 1147
- 1114 [39] Nasibov EN, Ulutagay G. Robustness of density-based cluster- 1148
- 1115 ing methods with various neighborhood relations. Fuzzy Sets 1149
- 1116 and Systems. 2009; 160(24): 3601-15. doi: 10.1016/j.fss.2009. 1150
- 1117 06.012. 1151
- 1118 [40] Bryant A, Cios K. RNN-DBSCAN: A density-based clustering 1152
- 1119 algorithm using reverse nearest neighbor density estimates. 1153
- 1120 IEEE Transactions on Knowledge and Data Engineering. 2018; 1154
- 1121 30(6): 1109-21. doi: 10.1109/tkde.2017.2787640. 1155
- 1122 [41] Hearn D. Computer graphics with OpenGL. New Delhi: Dor- 1156
- 1123 ling Kindersley India; 2014. 1157
- 1124 [42] Kostavelis I, Charalampous K, Gasteratos A, Tsotsos JK. 1158
- 1125 Robot navigation via spatial and temporal coherent seman- 1159
- 1126 tic maps. Engineering Applications of Artificial Intelligence. 1160
- 1127 2016; 48: 173-87. doi: 10.1016/j.engappai.2015.11.004. 1161
- 1128 [43] Aini A, Salehipour A. Speeding up the Floyd-Warshall algo- 1162
- 1129 rithm for the cycled shortest path problem. Applied Mathemat- 1163
- 1130 ics Letters. 2012; 25(1): 1-5. doi: 10.1016/j.aml.2011.06.008. 1164
- 1131 [44] Pradhan A, Mahinthakumar G. Finding all-pairs shortest 1165
- 1132 path for a large-scale transportation network using parallel 1166
- 1133 Floyd-Warshall and parallel Dijkstra algorithms. Journal of 1167
- 1134 Computing in Civil Engineering. 2013; 27(3): 263-73. doi: 1168
- 1135 10.1061/(asce)cp.1943-5487.0000220. 1169
- 1136 [45] Li W, Pu H, Schonfeld P, Zhang H, Zheng X. Methodol- 1170
- 1137 ogy for optimizing constrained 3-dimensional railway align- 1171
- 1138 ments in mountainous terrain. Transportation Research Part 1172
- 1139 C-emerging Technologies. 2016; 68: 549-65. doi: 10.1016/j. 1173
- 1140 trc.2016.05.010. 1174
- 1141 [46] Cui QL, Wu HN, Shen SL, Xu YS, Ye GL. Chinese karst 1175
- 1142 geology and measures to prevent geohazards during shield 1176
- 1177 tunnelling in karst region with caves. Natural Hazards. 2015; 1177
- 77(1): 129-52. doi: 10.1007/s11069-014-1585-6.
- [47] Alija S, Torrijo FJ, Quinta-Ferreira M. Geological engineer- 1145
- ing problems associated with tunnel construction in karst rock 1146
- masses: The case of Gavarres tunnel (Spain). Engineering Ge- 1147
- ology. 2013; 157: 103-11. doi: 10.1016/j.enggeo.2013.02.010. 1148
- [48] Zheng Y, He S, Yu Y, Zheng J, Zhu Y, Liu T. Characteristics, 1149
- challenges and countermeasures of giant karst cave: A case 1150
- study of Yujingshan tunnel in high-speed railway. Tunnelling 1151
- and Underground Space Technology. 2021; 114: 103988. doi: 1152
- 10.1016/j.tust.2021.103988. 1153
- [49] Fan H, Zhang Y, He S, Wang K, Wang X, Wang H. Hazards 1154
- and treatment of karst tunneling in Qinling-Daba mountainous 1155
- area: overview and lessons learnt from Yichang-Wanzhou rail- 1156
- way system. Environmental Earth Sciences. 2018; 77(19). doi: 1157
- 10.1007/s12665-018-7860-1. 1158
- [50] Kaufmann G, Romanov D. Modelling long-term and short- 1159
- term evolution of karst in vicinity of tunnels. Journal of Hydrol- 1160
- ogy. 2020; 581: 124282. doi: 10.1016/j.jhydrol.2019.124282. 1161
- [51] Park HS, Adeli H. Distributed neural dynamics algorithms 1162
- for optimization of large steel structures. Journal of Structural 1163
- Engineering. 1997; 123(7): 880-8. doi: 10.1061/(asce)0733- 1164
- 9445(1997)123:7(880). 1165
- [52] Siddique N, Hojjat Adeli. Harmony search algorithm and its 1166
- variants. International Journal of Pattern Recognition and Arti- 1167
- ficial Intelligence. 2015; 29(08): 1539001-1. doi: 10.1142/ 1168
- s0218001415390012. 1169
- [53] Siddique N, Adeli H. Simulated annealing, its variants and 1170
- engineering applications. International Journal on Artificial 1171
- Intelligence Tools. 2016; 25(06): 1630001. doi: 10.1142/ 1172
- s0218213016300015. 1173
- [54] Akhand MAH, Ayon SI, Shahriyar SA, Siddique N, Adeli H. 1174
- Discrete spider monkey optimization for travelling salesman 1175
- problem. Applied Soft Computing. 2020; 86: 105887. doi: 1176
- 10.1016/j.asoc.2019.105887. 1177